Sensors & Actuators: A. Physical 346 (2022) 113778

Contents lists available at ScienceDirect

Sensors and Actuators: A. Physical

journal homepage: www.journals.elsevier.com/sensors-and-actuators-a-physical

Fiber Bragg Grating Sensors ice detection: Methodologies and performance

M. Gonzalez *, M. Frövel

Instituto Nacional de Tecnica Aeroespacial (INTA), Carretera de Ajalvir km 4, Torrejon de Ardoz, 28850, Madrid, Spain

ARTICLE INFO

Keywords:
Ice detection
Icing
Optic Fiber
FBGS

ABSTRACT

New Researches have been done recently in order to create and adapt new systems to the recent Appendix O FAR 25 Aeronautical aircraft icing regulations. One important issue are the Supercooled Large Droplets (SLD) that are an important hazard in many cases. Novel sensor technologies for aircraft are being developed in order to assess the ice severity and to discriminate between large size droplets and small size droplets ice accretions.

The European SENS4ICE project gives founding for the research and development of several aeronautical ice detection systems that can discriminate between Appendix C and Appendix O conditions. In the present paper, the strengths and weaknesses of the Fiber Optic ice Detector (FOD) developed by INTA are discussed using a test matrix from the Canadian National Research Council (NRC). The FOD has presented good performance at the NRC ice wind tunnel tests in the ice detection time, detecting ice in most cases earlier than required by the actual standard (ED-103). Its lightness, low intrusiveness and small size, makes the FOD ideal for aeronautical applications. It measures indirectly the icing cloud characteristics, such as the liquid water content (LWC) and the ice accretion rate, so only an approximate severity assessment could be done.

1. Introduction

Several studies have treated the problem of ice in aircraft and the hazard that it represents. Many of them evaluated icing repercussions to the aircraft aerodynamic performance [1] and its effect to the aircraft efficiency and safety. The consequences of icing can be either an increase in energy consumption or a decrease in the operational safety. In order to ensure operational safety, an aircraft must be protected against a certain icing conditions envelope which is defined in the U.S. regulations 14 CFR Part 25 Appendix C [2] and Appendix O [3]. Appendix C indicate the probable maximum Liquid Water Content over a certain distance. In this Appendix, the Supercooled Large Droplets problem is not treated and it is only focused in small size droplets.

The Ice Protection System (IPS) should be activated only when ice accretion is produced in order to minimize energy consumption. It is important to have feasible Icing detection systems, that detect ice with a high accuracy and certainty in order to activate IPS only when it is necessary without compromising the operational safety [4].

In the past years one of the most important issues to be solved are the Supercooled Large Droplet (SLD) conditions. New regulations were introduced in 2014, in concrete appendix O in FAR 25 and CS-25. Appendix O add some requirements to the Ice Protection Systems, so the aircraft will be protected against Supercooled Large Droplets. When there are SLD conditions, the large droplets impinges more surface so ice is accreted in larger areas downstream the leading edge, so an adaptation to the normative is mandatory [5]. The regulation provides of an envelop in which the SLD conditions, Freezing Rain or Freezing Drizzle are more probable.

The new regulations need novel methods for the detection and protection of aerodynamic surfaces. For the adaptation of the new detection systems, several standards [6,7] that provide of certain requirements like Liquid Water Content or MVD measurement precision, detection time and so on were created. In concrete, EUROCAE ED-103, provides of a quite detailed guide of the current necessities in Ice Detection and interrogation. There are several topics like Detection parameters, Icing Wind Tunnel tests, Flight tests or Icing performance tests that are exposed in the standard. One of the main characteristics of EUROCAE ED-103 are its strict requirements for the detection, having to detect low Liquid Water Contents of 0,05 g/m3 in short times with very high measurement accuracy.

Those requirements cannot be satisfied by a single sensor. Furthermore, not only detection performance parameters are taken into account, other variables like size, weight, airflow invasion or robustness should be taken into consideration in a Primary Icing Detection System [6]. Additionally, sensors should satisfy other requirements in order to operate in an aircraft like altitude pressure, temperature, humidity, shock, vibration, abrasion, dust and so on. All those conditions and standardized tests are compiled in RTCA DO-160G [8] and in ED-103 as well.

* Corresponding author.
E-mail address: gonzalezvm@inta.es (M. Gonzalez).

https://doi.org/10.1016/j.sna.2022.113778
Received 11 May 2022; Received in revised form 21 July 2022; Accepted 22 July 2022
Available online 11 August 2022

There are many sensors with different operational principles Jackson and Goldberg [9], that can be applied to sense ice accretion or certain atmospheric conditions. In the SENS4ICE project frame, there are two types of FIDS, atmospheric or ice accretion sensors, which detect cloud conditions or ice thickness growing respectively. All sensors have certain advantages and disadvantages in its performance and its compatibility with the rest of the aircraft equipment. For safety issues, sensors must provide as much information as possible so a severity assessment could be made. Depending on the external detected conditions, different actions like IPS activation or route modification could be made. Optic Fiber sensors should be compared with sensors that operate with other sensor principles like pneumatic, magnetostrictive, piezostrictive, ultrasonic, dielectric, acoustic or microwave [10–13].

One of the detection principles gathered in [9] are the latent energy based sensors. Latent energy based sensors, detect the latent energy released by the supercooled water when it freezes and interpret the change in the heat flux on the surface as ice. Among the latent energy based sensors there are some sensors that detect a temperature difference between a reference and another temperature sensor [14], sensors that measure the heat required for heating a surface or wire [15], and sensors that measure the temperature heating curve of a heated wire (second type described in Jackson and Goldberg [9]). The optic fiber sensor developed by INTA [16,17] detects the surface temperature distribution and makes an assessment of the icing conditions.

There are many advantages of using an Optic Fiber Icing Detection system like lightness, non-susceptibility to electromagnetic interference or small size. This makes the optical fiber a powerful tool for ice detection. Many optic fiber sensors were created for FIDS like light scattering, photonic, fiber optic switch [18–20]. Additionally, Optic fibers could be used as a support in other sensors in which the temperature is a critical parameter, like Surface Acoustic Waves sensors.

2. Materials and methods

2.1. Fiber Bragg grating as a temperature sensor

Firstly, it is important to describe briefly all the components involved in the tests. One of them is the Fiber Bragg Grating Sensors (FBGSs) from the company FBGS INTERNATIONAL, manufactured with the Draw Tower process [21]. For a more detailed description Ref. [16] is recommended. The FBGS optic fiber sensors use the principle of Bragg reflection in a specific broadband that depends on magnitudes like temperature or strain. Eq. (1) shows a relationship between wavelength, temperature, strain (ε), refractive index (n) and grating period (Λ) [22]:

$$\lambda_B(\varepsilon, T) = 2n(T)\Lambda(T, \varepsilon) \quad (1)$$

In order to isolate the FBGS from strains (ε), the optic fiber was introduced in a capillary, so Eq. (1) can be simplified as a third degree polynomial function $T(\lambda_B) = a\lambda_B^3 + b\lambda_B^2 + c\lambda_B + d$ [22,23]. For the calibration, the instrumented airfoil was introduced in the temperature calibrator and three cycles with five temperature steps were applied between 20 °C and -30 °C.

As previously mentioned, for isolation reasons and to avoid any parasitic strain, the optic fiber is located in a freely movable manner inside a polyimide capillary. There is a gap between the fiber and the capillary, so all the external loads are supported by the capillary. Gratings are separated one centimeter each other and the width of the gratings is of approximately of 8 mm. The spectral response of the fiber can be seen in Fig. 1. The spectral response of the lower surface is weaker than the spectral response of the upper surface, but all peaks can be detected without problems. Both responses were represented for different temperatures, 22 °C and -15 °C. The spectrum peaks, and the scattered wavelengths have a displacement due to the temperature variations as it is indicated in Eq. (1).

The gratings are located along the airfoil chord, so the temperature profile could be measured easily. Horizontal positions from the leading edge of all the temperature sensors detailed in Table 1. In Fig. 2 is represented how the sensors are placed in the airfoil surface.

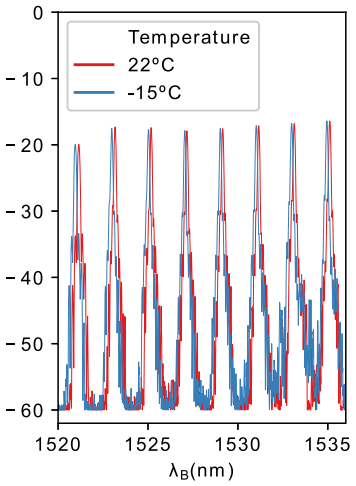

Fig. 1. Spectral response of the sensor for two different temperatures.

Table 1
Chordwise distance of each sensor from the leading edge.

Sensor	x (mm)
FBG15	0
FBG14	3
FBG13	10
FBG12	18
FBG11	27
FBG10	35
FBG9	46
FBG8	56

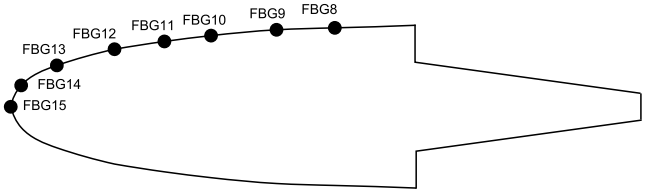

Fig. 2. Sensor Positions.

2.2. Tests descriptions

The sensor was tested in the NRC IWT, with the protocol defined by the SENS4ICE project. The testing protocol was based on the EUROCAE ED-103 standard. Conditions in CS-25 Appendix O and C were tested in order to see the sensor performance. The test procedure for both conditions is the following:

1. Start the data recording
2. Record data for 1 min in clear air
3. Start the icing cloud
4. Once an icing signal is detected, run for one minute
5. Stop the icing cloud

In the procedure, there is an aerodynamic conditions stabilization before the data recording and fogging. Some conditions were repeated because they were of special interest in order to be compared with other Icing Wind Tunnel results. It has been considered important to do more than one cycle of icing clouds in order to know how an ice layer

Table 2
Conditions tested in NRC: Liquid Water Content, Median Volume Diameter, Static Temperature, Airspeed, and type of the droplet population (Condition) are indicated for all tests.

Case	Condition	Airspeed [m/s]	Static [° C]	MVD [μm]	LWC [g/m^3]	Case	Condition	Airspeed [m/s]	Static [° C]	MVD [μm]	LWC [g/m^3]
1	LW-C CM	40,1	−20	15	0,3	19	LW-C IM	84,9	−3,5	35	1
2	LW-C CM	40,1	−10	20	0,42	20	unimodal	76,1	−17,7	163,5	0,82
3	LW-C CM	84,9	−10	23	0,34	21	unimodal	40,1	−17,7	122	0,46
4	LW-C CM	40,1	0	23	0,54	22	LW-FZDZ	79,7	−20	106	0,4
5	LW-C CM	84,9	−20	30	0,11	23	LW-FZDZ	79,7	−25	20	0,29
6	LW-C CM	84,9	−10	40	0,1	24	LW-FZDZ	84,9	−15	20	0,35
7	LW-C CM	84,9	−10	35	0,15	25	LW-FZDZ	84,9	−10	20	0,38
8	LW-C CM	84,9	−30	35	0,05	26	LW-FZDZ	84,9	−3,5	20	0,42
9	LW-C CM	84,9	−3,5	30	0,35	27	LW-FZDZ	84,9	−25	20	0,15
10	LW-C IM	40,1	−20	22	1,5	28	LW-FZDZ	84,9	−15	20	0,18
11	LW-C IM	40,1	−10	28	1,2	29	LW-FZDZ	84,9	−10	20	0,2
12	LW-C IM	84,9	−20	23	1,3	30	LW-FZDZ	84,9	−3,5	20	0,21
13	LW-C IM	40,1	−20	42	0,3	31	LW-FZDZ	84,9	−25	110	0,18
14	LW-C IM	84,9	−20	20	1,75	32	LW-FZDZ	84,9	−15	110	0,22
15	LW-C IM	84,9	−10	20	2,25	33	LW-FZDZ	84,9	−10	110	0,23
16	LW-C IM	84,9	−10	20	0,5	34	LW-FZDZ	84,9	−3,5	110	0,26
17	LW-C IM	84,9	−20	31	0,75	35	unimodal	84,9	−10	180	0,25
18	LW-C IM	84,9	0	20	2,5	36	unimodal	84,9	−10	220	0,25

accreted in the surface affects to the detection. The icing cycle duration was of two minutes in order to check if there are any false negatives during the ice accretion. The FIDS has to detect the icing cloud ending before a certain time that is according to SAE AS5498 of 3 min . The ice off signal detection time could be important in an operational context due to the cost savings in Ice Protection Systems.

Test conditions are gathered in Table 2. Those conditions, were carefully chosen in order to evaluate the performance of the different SENS4ICE sensors. Each condition is critical and it is tested in order to corroborate if a certain sensor can be operative in FAR 25 Appendix C and O conditions limits envelope. The table shows conditions that have different restrictions like Liquid Water Content (case 8 for low water content and case 18 high water content), temperatures (test case 18 for high temperatures or for low temperatures case 18) or airspeed (40 m/s or 85 m/s). There are conditions that represent all the cases in FAR 25 Appendix C Continuous maximum (CM) and Intermittent Maximum (IM) and Appendix O Freezing Drizzle (FZDZ). Normally, the Large Droplet populations should show a bimodal distribution, having a ratio of small droplets. In some tests, instead of a bimodal, the droplet distribution is unimodal, being the majority of the droplets large. In those cases the effect of the droplet size in the ice accretion is more accentuated.

The testing procedure could be seen in Fig. 3 were is represented the fiber temperatures of the airfoil along the chord. It can be seen that the farther the sensor is from the leading edge, the lower is the temperature step. This is because there are more supercooled droplets impacting the area close to the leading edge and because during ice accretion, the air is more turbulent in the back part of the airfoil, and the turbulence increases the convection loss. The sensor should detect ice formation before a certain response time. The response time is function of a maximum allowable ice thickness τ which is normally 0.3 mm, the collection efficiency in the stagnation point β, the Liquid Water Content LWC and the freezing fraction η, and the time t:

$$\tau = t\frac{\rho}{\beta_0 LWCV\eta} \tag{2}$$

In EUROCAE ED-103, there is a detailed guide of the sensor performance characteristics that should be evaluated. In first place, according to that standard, is important to detect (interrogate) Liquid Water presence for LWC higher than 0.05 g/m3. When Ice is detected, the FIDS should discriminate and show to the crew if the aircraft is flying in Appendix C or Appendix O conditions. If it is flying in Appendix O conditions, for safety reasons, it is important that the FIDS can discriminate between Drizzle and Rain, giving a warning to the crew. The standard recommend to detect some additional parameters that can give information of the severity like LWC, MVD or Ice Accretion Rate (or other like ice thickness or maximum droplet diameter).

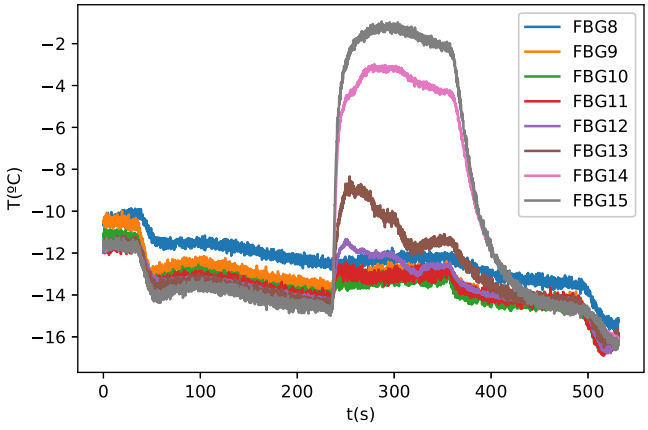

Fig. 3. Test temperature profile example.

2.3. Detection methodologies

As it can be seen in Fig. 3 and in Ref. [16], there is a temperature step in the sensor signal which depends on the grating position. This temperature step is caused by a new energetic equilibrium produced by the Liquid Water impacting the airfoil surface. Several methods could be used in order to detect ice presence. Firstly, a method could consist on measuring the temperature difference between a detection grating, which is exposed to Liquid Water, and a reference grating, which is not. This method is used in several systems for LWC and TWC measurements like Nevzorov probe [15] or other hot wire probes. In this case, this kind of detection principle is not sufficiently accurate for ice detection in the airfoil, because there are many false positives caused by surface heterogeneities along the surface when there are changes in the airspeed or in the total temperature.

The nature of the signal temperature rising when an icing event occur is abrupt, so this fact could be used for ice detection. One variable that is useful to detect the abruptness of the icing signal is the temporal first derivative of the temperature difference between a detection sensor and a reference sensor FBG8(see Fig. 4). The temperature signal is quite noisy so a previous signal filtering should be applied, and then the temporal derivative is calculated through finite differences. There are many filters which can be useful, but Savitzky–Golay filtering [24] was applied due to its simplicity. Once the first derivative is calculated, ice detection occurs when the temperature first temporal derivative is over a certain threshold. The problem of this method is the computational cost of the filtering and later derivative calculation.

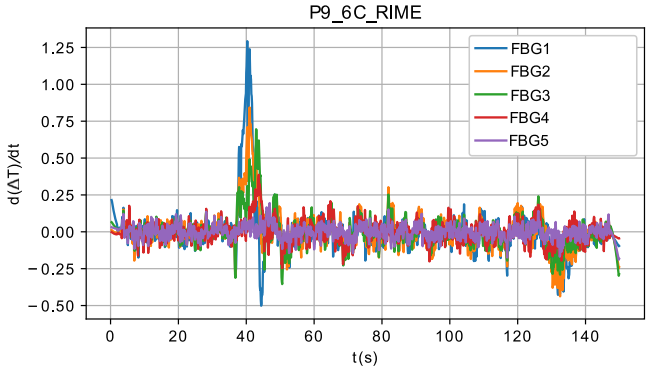

Fig. 4. Temperature temporal first derivative Example.

2.4. Discrete wavelet transform

Other Filtering and Ice Accretion Detection method could be using Discrete Wavelet Transforms. The Discrete Wavelet Transform is used in several applications like Image processing or data extraction. In fiber sensing has been used a lot for FBGs and interferometric sensors [25]. In this case it could be very useful because the signal can be filtered and the abrupt changes can be detected directly.

When a wavelet transform is applied a signal is mapped with a function that depends on scaling (a) and shift (b) parameters. That mapping signal is defined by a kernel function (Eq. (3)). All kernel functions have in common that have its maximum in $\psi(0)$ and is null in $\lim_{x\to\pm\infty}\psi(x)$. For this reason, Wavelets can be very useful for detecting and categorizing transitory events in the signal. There are several types of wavelets that could be used like Daubechies, Biorthogonal, Coiflets, Mexican Hat, and so on. In this work the Haar function has been used due to its simplicity and usefulness.

$$\psi_{ab}(t) = \frac{1}{\sqrt{a}}\psi\left(\frac{t-b}{a}\right) \tag{3}$$

In the case of DWT, normally another parameters different than the previous a and b are used. Applying the procedure for continuous-time analog signals in Ref. [26], and considering $a_0 = a^{-m}$ and $b_0 = b(na)^{-1}$, the discrete wavelet transform basis, m the level and n an index that designates the wavelet:

$$\{\psi_{mn}\} = a_0^{-m/2}\psi(a_0^{-m}t - nb_0) \tag{4}$$

The treated function, in this case the temperature difference between the detection and reference grating ΔT, could be expressed as the superposition of the kernel function of Eq. (4) and the DWT coefficients $d_{m,n}$:

$$\Delta T = \sum_{m=0}^{\infty}\sum_{n=-\infty}^{\infty} d_{m,n}\psi_{mn} \tag{5}$$

The wavelets coefficient $d_{m,n}$ gives information of certain events in the signal. In this case, the scaling parameter a, represents how abrupt is the change of the signal and the shift parameter b represents the moment when it happens. Those parameters are discretize with the natural numbers n and m. The signal would be, the sum of the contribution of all the wavelets and its coefficient. When an abrupt event happens in the signal, the coefficient in that moment has a higher absolute value for a specific scale factor. The coefficients are calculated through a convolution:

$$d_{m,n} = a_0^{-m/2}\int_{-\infty}^{+\infty} f(t)\psi(a_0^{-m}t - nb_0)dt \tag{6}$$

The advantage of the Haar kernel function $\psi(t)$ is its simplicity, because its values are 1 for $0 \le t < 1/2$, -1 for $1/2 \le t \le 1$ and null for the rest of the t values. This fact makes more simple Eq. (6). In the case of the Haar kernel function $\psi(t)$, the discrete parameters from Eq. (4) are $a_0 = 2$ and $b_0 = 1$, so the integral could be simplified as:

$$d_{m,n} = 2^{-m/2}\left[\int_{2^m n}^{2^m(1/2+n)} \Delta T(t)dt - \int_{2^m(1/2+n)}^{2^m(1+n)} \Delta T(t)dt\right] \tag{7}$$

The function ΔT is discrete in this case, so the continuous time and temperature signals could be discretize as a function of the sampling time T_s.:

$$\begin{aligned} t_i &= T_s i \quad i \in \mathbb{N} \\ \Delta T_i &= \Delta T(t_i) \end{aligned} \tag{8}$$

Solving Eq. (7) with the previous discretization, the result is:

$$d_{m,n} = 2^{-m/2}\left[\sum_{i=(2^m n)/T_s}^{\frac{2^m(1/2+n)}{T_s}} T_s\Delta T_i - \sum_{\frac{2^m(1/2+n)}{T_s}}^{2^m(1+n)/T_s} T_s\Delta T_i\right] \tag{9}$$

2.5. Wavelet construction

A complementary basis to the band-pass wavelets, a low pass function $\phi(t)$ called scaling function is used. This function satisfy the orthonormal condition:

$$\int \phi_{mn}(t)\phi_{ms}(t)dt = \delta_{ns} \tag{10}$$

The values of the scale functions coefficients are obtained by a similar process than with the $d_{m,n}$ coefficients (Eq. (6)):

$$\begin{aligned} c_{m,n} &= a_0^{-m/2}\int_{-\infty}^{+\infty} \Delta T\phi(a_0^{-m}t - nb_0)dt = \\ &= 2^{-m/2}\int_{2^m n}^{2^m(1+n)} \Delta T(t)dt = 2^{-m/2}\int_{i=2^m n}^{2^m(1+n)} T_s\Delta T_i \end{aligned} \tag{11}$$

The complementary scale function is used for avoiding to express the function in Eq. (11) with infinite wavelet band pass functions. The function ΔT in the level L would be expressed as a decomposition of the lower resolution of the scaling basis and the approximation error represented by the term $\sum_{m=0}^{L}\sum_{n=-\infty}^{\infty} d_{m,n}\psi_{mn}$.

$$\Delta T_i = \sum_{n=-\infty}^{+\infty} c_{L,n}2^{-L/2}\phi\left(\frac{t}{2^L} - n\right) + \sum_{m=0}^{L}\sum_{n=-\infty}^{\infty} d_{m,n}\psi_{mn} \tag{12}$$

2.6. Representation of an icing test using wavelets

The Discrete Wavelet Transform acts like a filter bank [27]. The functions can be decomposed by a scaling bases (first term in Eq. (12)) and an approximation error (second term in Eq. (12)) . Each level m represents one more filtering step in the filter bank. Filter Banks could be used for categorizing the signal changes in function of its abruptness depending on the level that is applied. In this case, the surface temperature rising is abrupt when fogging starts, so this temperature change could be detected and categorized easily with wavelets.

Many levels could be used for the fogging beginning detection but the sixth has shown the best performance according to the NRC test results. Some tests with high instabilities like high air turbulence or very high Liquid Water Content variations show that the sixth level could be too much sensible, but the ratio between sensibility and specificity has been considered the best. In Fig. 5,it can be seen filtered signal for the fourth, fifth and sixth level. In this case a higher level means a more accentuated signal filtering.

The kernel function coefficients $d_{m,n}$, were considered as representative of the icing events. In Fig. 6 are represented the different coefficients of a test in the last three levels. The coefficient values were normalized as $d_{m,n}2^{-m/2}$. It can be seen that the fogging beginning can be easily located in the second 230, due to the abrupt temperature change. The time in level m can be calculated from the n values:

$$t_{m,n} = n2^m T_s \tag{13}$$

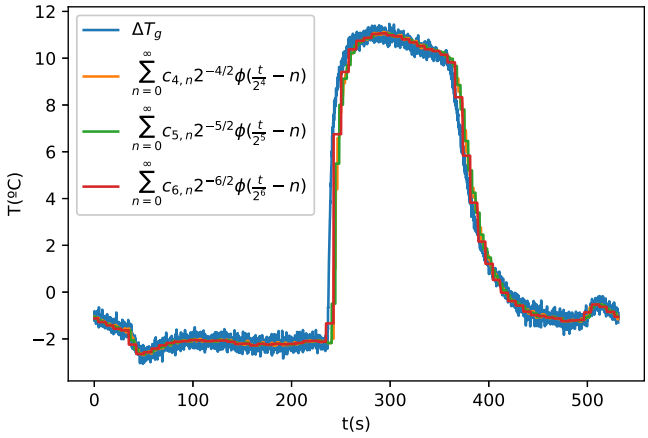

Fig. 5. Filtered temperature signal for three different levels (4, 5 and 6).

In Fig. 6 can be seen that higher the DWT levels m imply less dimension in the $d_{m,n}$ coefficient. The integral of Eq. (6) is between $2^m n$ and $2^m(1+n)$, so higher levels need more quantity of samples in order to calculate the coefficients. This fact could affect to the detection time because the higher is the interval in order to calculate the coefficients, the lower is the precision for knowing when the ice accretion begins.

For the discrimination between ice accretion presence and ice accretion absence, a detection threshold is used. In this case, the detection threshold will be selected according to parameters like heights and prominences of the peaks in the Discrete Wavelet Transform (see Fig. 6).

In Fig. 6 can be noted that the detection is quite efficient and intuitive. In this particular test, all levels would detect the fogging beginning but only the sixth level would be enough to detect the end of the fogging. In other tests the Liquid Water Content is not so high, so the ice detection is not guaranteed in the fourth and fifth levels neither. This method has been probed as very effective in order to quantify the abruptness of the temperature rising and to discriminate other events like flow acceleration, temperature changes or high LWC variations.

Another advantage of using DWT is the filtering and data reduction of the signal(Fig. 5). This makes easier to process the data of the signal in order to estimate important variables like the Ice Accretion Rate and Liquid Water Content (Sections 2.9 and 2.10). These variables are very interesting to know, for detection issues or for knowing the severity of the icing conditions.

The system was designed to evaluate the signal in real time so an online algorithm was implemented. The evaluation takes the last 300 s of data and calculates the Discrete Wavelet Transform DWT of the signal. In the moment that detects ice, the algorithm begins a sub process that calculates the Liquid Water Content and Ice accretion rate using the temperature profile on the airfoil surface. Each 3 s the signal has to be refreshed and DWT must be calculated again. The refresh time was set in three seconds because the most severe condition in ED-103, has a detection time of 3 s.

As it can be seen in Section 2.3, in the beginning of the SENS4ICE project an algorithm that smooths the signal and detects ice accretion through the first temporal derivative of the signal was designed. The computational cost of smoothing and then calculating the derivative with finite differences was too high so that idea was rejected. Discrete Wavelet Transform analysis has been proven as a very fast method for the data processing. This is very important in order to apply a real time detection algorithm.

Before NRC tests, several Icing Wind Tunnel tests were carried out in INTA IWT in order to test the sensor. The conditions tested in INTA could be seen in Ref. [16]. The algorithm was effective in a LWC 0,3 g/m3 to 1 g/m3 range. Additionally, the tests were done with different angles of attack, for demonstrating the feasibility of the system.

2.7. Detection process

In Fig. 7 can be seen the algorithm used for detecting ice in real time. This process is done each 3 s. In parallel of this process there is a data acquisition program in which the peaks of the wavelength are calculated and transformed to temperatures with a calibrated cubic regression (Section 2.1). The temperature difference between the sensor located in the leading edge and a reference sensor located in the trailing edge is calculated. The wavelet transform in made from that difference and after the threshold is calculated using the expression from Section 2.8.

The program was made in Python, and the *scipy* function find_peaks function was used in order to detect Liquid Water presence. The function gives as a result a list of samples which prominence are higher than the threshold previously calculated. Knowing the time when the ice is detected after the wavelet transform is done is not so straightforward, because a data reduction is done. The calculated time is taken from the expression (13).

The program detects two peaks, one of them is used to know when the fogging cycle begins and the other one is used to know when it finishes:

- The peaks bigger than the threshold in the function $d_{m,n}$, are the no ice peaks (positive peaks)
- The peaks bigger than the threshold in the function $-d_{m,n}$, are the no ice peaks (negative peaks)

Finally the detection algorithm contemplates the following four possibilities:

(1) If the number of ice peaks detected are zero, there is not ice.
(2) If the number of ice peaks detected is not zero, but the number of no ice peaks is zero, then there is Ice.
(3) If the time of the last ice peak is bigger than the last no ice peak, then there is ice, because there is an ice peak detected after the last fogging ending.
(4) If the previous conditions are false, there is not ice. This means that there is a no ice peak detected after an *ice peak*. There is a fogging ending after the ice was detected so the algorithm would interpret that the fogging cycle has ended.

2.8. Threshold determination

Two different strategies were used in order to determine the ice detection and the ice stopping thresholds. The first strategy consist in select constant thresholds and study the specificity and sensibility of the sensor. With both variables, ROC curves could be calculated with an iterative process and then, select the specificity and sensibility that should be used [28].

The problem of this method is that it is not optimal because it does not take into account external effects that could be influential in the temperature rising abruptness like airspeed or total temperature. A possible solution is to use variable thresholds that depend on the temperature and airspeed:

$$Threshold(T_t, V) = a + bV + cT_t \tag{14}$$

For maximizing the performance of the threshold, a genetic optimization algorithm was used, in concrete it was used the Python function *optimize.differential_evolution* from the package *scipy*. For defining a optimization problem an objective function f should be defined. In this case, the objective function was the following:

$$f(a,b,c) = FP(a,b,c) - TP(a,b,c) \tag{15}$$

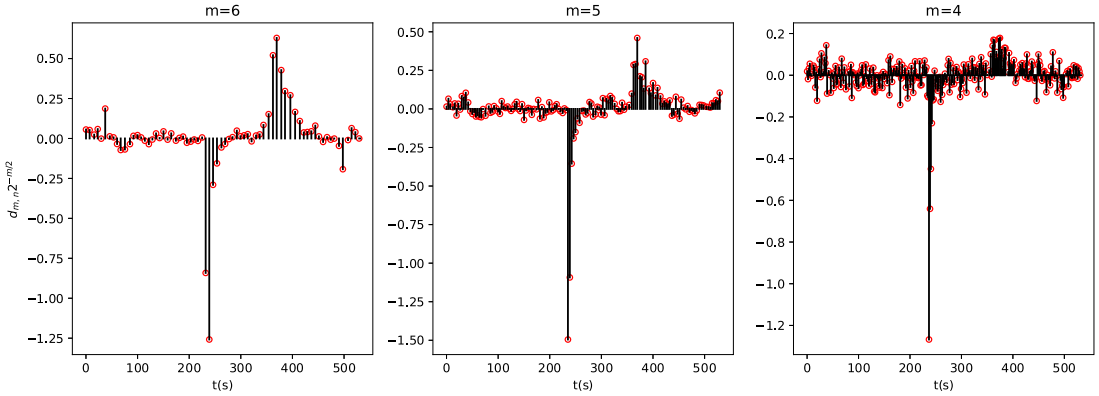

Fig. 6. Discrete wavelet coefficients of a test.

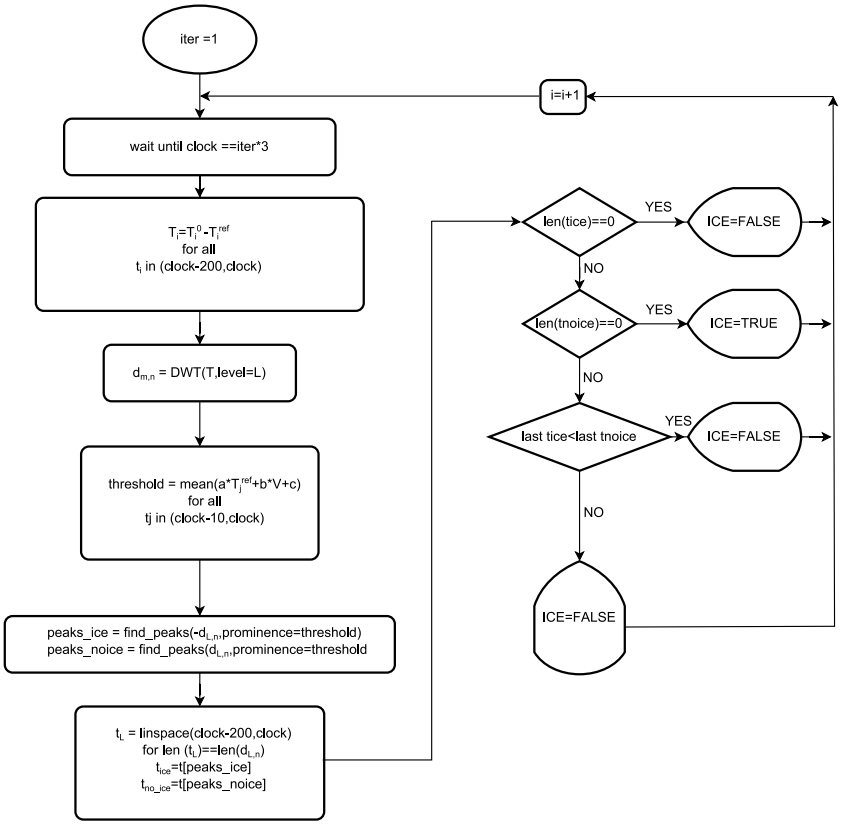

Fig. 7. Detection Algorithm Flowchart.

With Eq. (15) objective function, a compromise solution between sensibility represented by the True Positives (TP) and specificity represented by the False Positives (FP) is achieved. The optimization algorithm calculates the a, b and c values that minimizes f, finding the optimal parameters for the threshold function in Eq. (14). In order to determine the TP and FP, is important to establish a relationship between the threshold function in Eq. (14) and the TP and FP functions in Eq. (15). The followed procedure of that relationship is:

1. Coefficients $d_{6,n}$ were calculated applying the Discrete Wavelet Transform (DWT)
2. Each $d_{6,n}$ coefficient was associated with a timestamp. The fogging beginning timestamp is provided by NRC as well, so an matching between fogging parameters and wavelet coefficients can be done.
3. Determine which $d_{6,n}$ have a prominence below the detection fogging starting threshold $Th_{start}(a,b,c)$ and above the fogging stopping threshold $Th_{stop}(a,b,c)$. The times associated with those coefficients are saved in variables called t_{start} for the coefficients below the detection fogging starting threshold and t_{stop} for the coefficients above the fogging stopping threshold.

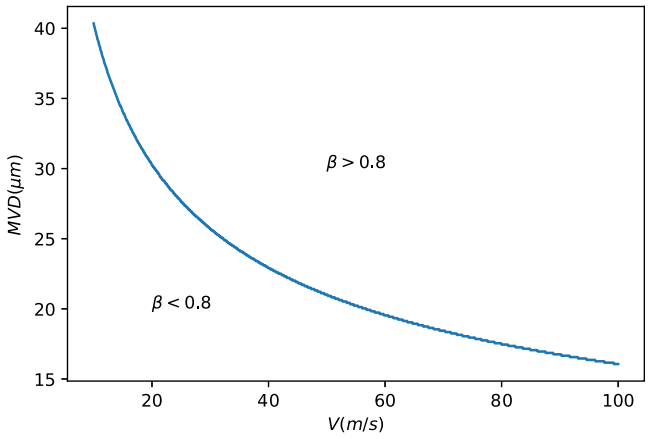

Fig. 8. Collection Efficiency as a function of the airspeed and MVD.

4. The data provided by NRC is compared with each detected t_{start} and t_{stop}. If the difference between t_{start} and the truth fogging beginning is less than 6 s, the algorithm considered that detected peak as a True Positive and if is greater or equal than 6 is considered as a False Positive.

2.9. LWC determination

In order to evaluate the severity of ice, an important parameter is the Liquid Water Content. LWC was calculated with a Messinger model [29], using a heat balance with the temperature data as it is described in Ref. [16] as it can be seen in Eq. (16). The collection efficiency in the stagnation line β_0 could be calculated or numerically or analytically with the Langmuir Blodgett method [30].

$$\dot{m}^0_{im} = \frac{h^0(T^0_{sur}-T^0_{rec})}{c^0_{p,is}(T^0_{sur}-T_{mp})+\frac{V^2_\infty}{2}+L^0_f-c^0_{pw}(T_{mp}-T_\infty)}$$
$$LWC = \frac{\dot{m}^0_{im}}{V\beta_0} \tag{16}$$

Using this expression has several problems in order to determine the LWC. In first place, the convective heat transfer coefficient is difficult to estimate analytically in a feasible way [31,32]. Many times, the leading edge of the airfoil could be consider as a cylinder [33], and the convective heat transfer coefficient could be calculated with the expression in Eq. (17) [34]. Another issue that should be taken into account is that the value of the convective heat transfer coefficient depends on the roughness [35,36] and the separation point. Both parameters change during the ice accretion [37], so it is difficult to establish an analytical and constant value of the heat transfer coefficient.

$$h_c = 1.14\left(\frac{\rho_a V_\infty D}{\mu_a}\right)^{0.5} Pr^{0.4}\frac{k_a}{D} \tag{17}$$

On the other hand, another source of error is the freezing fraction f. The Freezing fraction calculation is indirect, and should be calculated from other variables. It was defined by Messinger [29][38] and it has been used for ice accretion predictions in software like LEWICE [37,39]. If the ice is rime, the freezing fraction is the unity but in other cases is less than one. In the algorithm, the freezing fraction is considered as one and this makes the LWC prediction for rime ice more accurate than for glaze ice (see Fig. 12).

Lastly, another source of error is the collection efficiency. The collection efficiency depends on the airfoil geometry, the speed and the droplet size [30]. For the collection efficiency calculation, Lagrangian [37,39] or Eulerian [40,41] methods could be used. Analytically, collection efficiency could be calculated considering the airfoil leading edge as a cylinder and using equations described in [30,42]. Using those analytical expressions, the points in which the collection efficiency is equal to 0.8 for each droplet size and air speed was calculated.

Collection Efficiency has been considered as 0.9, because at high velocities (see Fig. 8) the collection in the leading edge does not suffer big variations, being its value close to the unity. For predicting the Liquid Water Content it is necessary to take the airspeed as an input. The temperature of the surface and the recovery temperature are taken from the FBGS data.

2.10. Ice accretion rate determination

The Ice Accretion Rate in the stagnation point is estimated in a similarly than the Liquid Water Content, in an equation that is also in the Ref. [16]:

$$\frac{d\Delta}{d\tau} = \frac{h^0(T^0_{sur}-T^0_{rec})}{\rho_{ice}\left(c^0_{p,is}(T^0_{sur}-T_{mp})+\frac{V^2_\infty}{2}+L^0_f-c^0_{pw}(T_{mp}-T_\infty)\right)} \tag{18}$$

The ice accretion rate is difficult to measure, and is very dependent on the ice density. The ice density can vary from 0.3 to 0.912 g/m3 [43,44], so the error that can committed could be quite big. LEWICE and other software, or standards like ED-103 consider the ice density as 0.880 g/m3 in case of rime, so that density was used. The other source of error in the ice accretion rate is the convective heat transfer coefficient on the leading edge as it is described in the previous section.

The same expression as applied in the stagnation point sensor (Eq. (18)) could be used in order to calculate the ice accretion rate in sensors located downstream the leading edge. For determining the Ice Accretion Rate, laminar flow is considered for simplicity reasons. The convective heat transfer coefficient rises downstream the separation point, so the ice accretion is underrated in backward regions. The density varies as well with the position, decreasing if the ice is rime (freezing fraction equal to one) and being constant if the ice is glaze (freezing fraction less than the unity).

3. Results

In this section the results presented are oriented in evaluating the sensor performance. There are many performance characteristics that should be studied. In first place the sensor temporal response for liquid water starting and exit. Secondly the accuracy for Liquid Water Content and finally the accuracy for Ice Accretion Rate.

3.1. Sensor detection

Using the threshold calculated in Section 2.8, sensor detection results are summarized in Table 3. Only in test cases 4, 9, 18 and 19 there is not ice accretion detection by the sensor. As can be seen in Fig. 9, no ice is formed in test 4 and 18. This makes them True Negative even though there is no detection. Test 4 was run 3 times without ice accretion and ice detection in any of the three repetitions.

On the other hand, the rest of the tests had ice accretion without detection, so all of them are false negatives. Looking at the Table 3, tests 4,9,18 and 19 have static temperatures close to 0 °C. The sensor response in those cases is somewhat particular as can be seen in Fig. 10. In all these cases the temperature drops initially and then rises to the initial temperature. This event could be caused due to the fact that the water is at the static temperature which is lower than the temperature of the airfoil surface. Therefore, the water cools down the airfoil lowering its temperature.

Test cases 9 and 19 have different responses than cases 4 and 18, as can be seen in Fig. 10. When fogging starts at t=0, it is noticed that whether there is ice accretion or not, the temperature drops. On the other hand, as soon as fogging ceases, a thermal drop is observed

(a) (b)

Fig. 9. Test cases without Ice accretion.**(a)** Test case 18.**(b)** Test case 4.

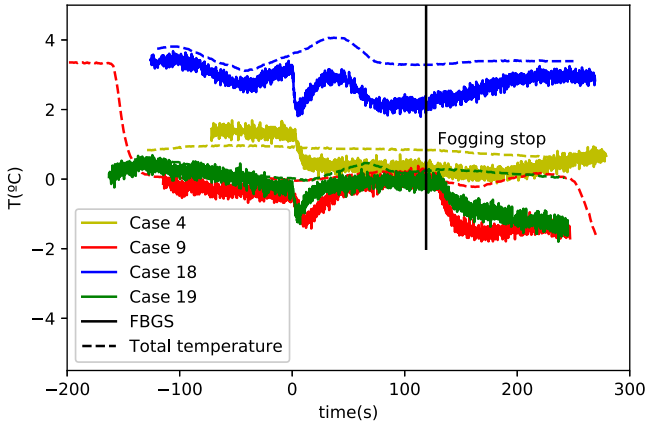

Fig. 10. Temperatures during the tests in which there is not ice detection.

Table 3
Detection results in test Matrix.

Case	Detection	Case	Detection	Case	Detection	Case	Detection
1	Y	10	Y	19	N	28	Y
2	Y	11	Y	20	Y	29	Y
3	Y	12	Y	21	Y	30	Y
4	N	13	Y	22	Y	31	Y
5	Y	14	Y	23	Y	32	Y
6	Y	15	Y	24	Y	33	Y
7	Y	16	Y	25	Y	34	Y
8	Y	17	Y	26	Y	35	Y
9	N	18	N	27	Y	36	Y

in tests 9 and 19, which is typical of purely rime conditions. This temperature drop indicates that latent energy has been present during fogging and that once fogging stops, the equilibrium temperature drops. In test cases 4 and 18, it can be observed that the temperature follows a similar pattern to the total temperature and that the temperature does not decrease when the fogging stops.

3.2. Sensor temporal response

The sensor temporal response was evaluated with the NRC test FBGS temperature data. The tests were simulated a posteriori, so the sensing parameters could be optimize. The algorithm was run in order to detect ice accretion each 3 s, like it is explained in Section 2.2. The algorithm output was saved and the time response was compared with ED-103 Requirements (Eq. (2)). The Optic fiber sensor has a very fast response but the algorithm many times does not interpret the temperature rising as ice until a certain time has passed. The bigger is the LWC and air speed, the higher is the latent energy released and this makes the temperature rising more abrupt. This fact makes the sensor faster with higher (LWC V) which normally implies more severe events.

Fig. 11 represents the sensor responses of all tests compared with ED-103 (red line) required response. The sensor normally satisfies ED-103 requirements with higher LWC, having much faster responses with lower Liquid Water Contents. Only cases 17 and 12 do not meet the strict temporal response ED-103 requirements (Eq. (2)), due to the algorithm refresh time of three seconds.

3.3. LWC accuracy

In the case of LWC, Eq. (16) was used and algorithm results were compared with NRC test data. In Fig. 12 results between data provided by NRC is compared with the measurements provided by the sensor. For understanding why results are not accurate for some LWC it is convenient to define the Ludlam limit as the $LWC\ V$ that makes the surface temperature reach 0 °C. Therefore, $LWC\ V$ values above the Ludham limit would produce freezing fractions less than one and the ice would be glaze. The following equation has been used in order to discriminate the tests between rime and glaze. If $(LWC \times V)_{Ludlam} < (LWC \times V)$ the ice is rime and else is glaze.

$$(LWC \times V)_{Ludlam} = \frac{h^0(T_f - T^0_{rec})}{\beta_0 \left(c^0_{p,is}(T^0_{sur} - T_{mp}) + \frac{V^2_\infty}{2} + L^0_f - c^0_{pw}(T_{mp} - T_\infty) \right)} \tag{19}$$

It can be seen the higher is the LWC, the lower is the accuracy of the sensor. It is because initially a freezing fraction value has been considered as one, and for glaze results freezing fractions are lower. The average error value has been 39% including glaze ice results. The error may be considered quite high but normally LWC are difficult to measure exactly. For example, according to Ice Tunnels Standard SAE ARP 5905 [45]: *"the uniform icing cloud is defined as the area of the test section over which the LWC does not vary by more than a ±20% from the test section centerline LWC value"*.

3.4. Ice accretion rate results

In case of the ice accretion rate, the value was not implemented but there is an error of a 42%. That error is not accurate neither because the reference value provided by the SENS4ICE project is an approximation as well, but it gives a representative value of the ice accreted in the leading edge. A more realistic accuracy values of ice accretion rate were exposed in Ref. [16] but with a test matrix more limited. Logically, the ice accretion rate should have higher precision because is not freezing fraction dependent.

3.5. Endurance tests

A long endurance test was made in order to evaluate the sensor response to long ice exposures. The main goal is to assess if the system can maintain its functionality over long periods of time. The temperatures and test DWT are shown in Fig. 13(b). The temperature

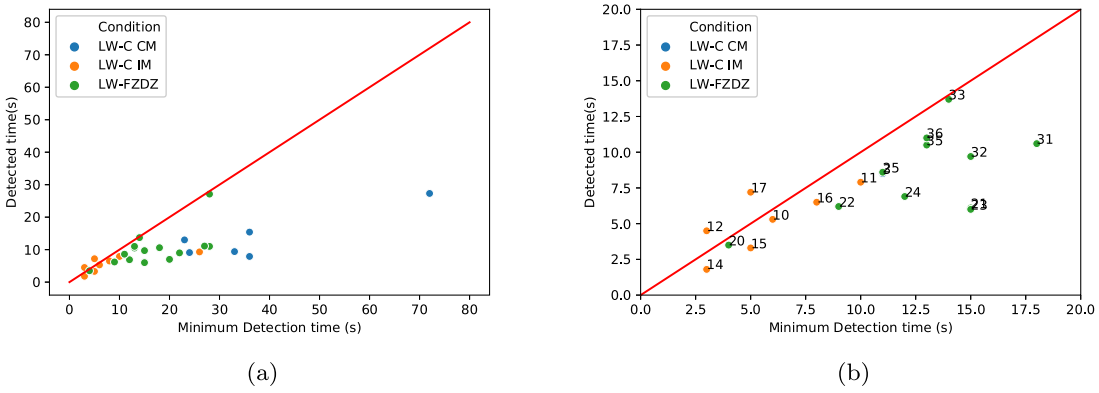

Fig. 11. Sensor Temporal Response for each condition.

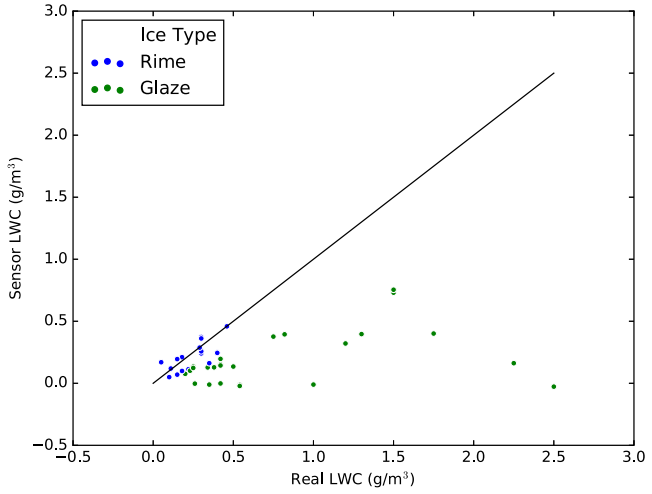

Fig. 12. Comparison between real and measured LWC.

remains quite stable after fogging so visually it is easy to identify the fogging existence, as it can be seen in sub Fig. 13(a). The beginning of the fogging cycle is easy to detect, but in the ending, due to the thickness of the ice layer, the temperature dropping is not enough abrupt to be detected (sub Fig. 13(a)).

Another level could be selected, with a different threshold, but it has been considered that it would imply a high quantity of false positives, so that option was not been taken into consideration. Even thought, the sensor performance is acceptable in order to detect ice for long ice exposures, but for detecting the fogging ending, the ice layer isolates the airfoil surface too much (see Fig. 14).

4. Conclusions

In this work the performance of an icing sensor based on Fiber Bragg Gratings has been studied according to the SENS4ICE and ED-103 standards. Several conditions were tested in NRC Icing Wind Tunnel in order to see how the sensor works in many different environments. A detection algorithm based on Discrete Wavelet Transform has been implemented and studied.

The system showed good detection results for different Liquid Water Content, airspeeds and MVD conditions in rime ice. For glaze ice conditions with temperatures close to 0 °C the results worst, showing two false negatives. The algorithm showed a very fast response, according to the ED-103, with different response times depending on the Liquid Water Content conditions. Only two tests had temporal responses slightly slower than the ED-103 standard. The algorithm has good results in detecting the fogging termination as well if the ice layer is not too thick.

The algorithm tried to measured the Liquid Water Content and Ice accretion rate in the surface. Results show a low accuracy in the LWC measurement in glaze ice conditions, but a higher one in rime ice. Ice Accretion Rate does not give a accurate result neither, probably because its difficult to give a trustful measurement of the ice layer thickness during the test. Finally, endurance test show that the temperature steps are present for long times, but if the ice layer is too thick, the sensor cannot detect the fogging termination.

Funding

This project has received funding from the European Union's Horizon 2020 research and innovation programme under grant agreement N° 824253.

CRediT authorship contribution statement

M. Gonzalez: Conceptualization, Methodology, Software, Data post-processing, Writing, Editing, Investigation. **M. Frövel:** Validation, Supervision, Investigation, Conceptualization.

Declaration of competing interest

One or more of the authors of this paper have disclosed potential or pertinent conflicts of interest, which may include receipt of payment, either direct or indirect, institutional support, or association with an entity in the biomedical field which may be perceived to have potential conflict of interest with this work. For full disclosure statements refer to https://doi.org/10.1016/j.sna.2022.113778.Malte Frovel reports financial support was provided by Horizon 2020. Malte Frovel has patent System and method for detecting ice formation on a body pending to ES WO2020053202A1.

Data availability

The authors do not have permission to share data.

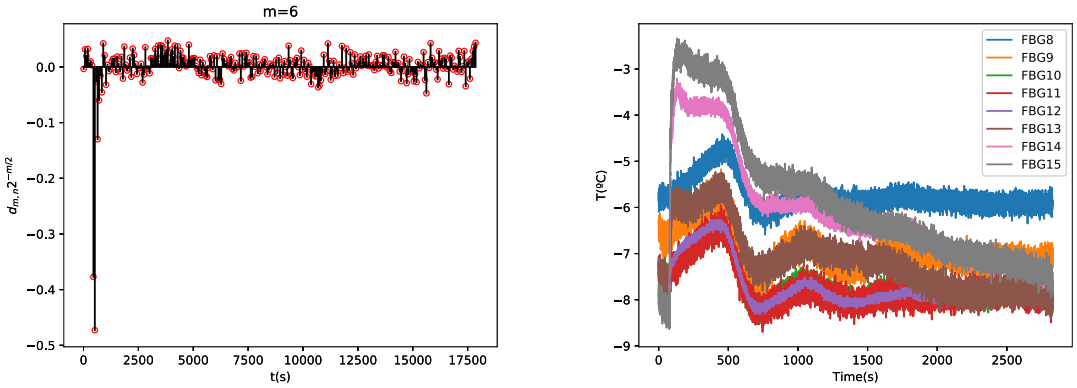

Fig. 13. Endurance test Results. (a) Discrete wavelet coefficients. (b) Temperature during the test.

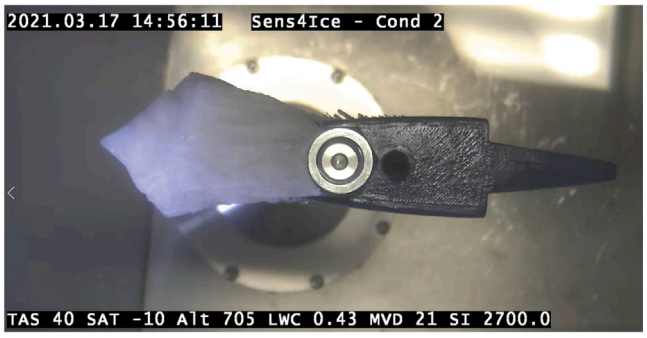

Fig. 14. Picture taken in the end of the endurance test.

References

[1] Y. Cao, W. Tan, Z. Wu, Aircraft icing: An ongoing threat to aviation safety, Aerosp. Sci. Technol. 75 (2018) 353–385.

[2] Federal Aviation Administration (FAA). 14 CFR Appendix C to Part 25.

[3] Federal Aviation Administration (FAA), 2016, 14 CFR Appendix O to Part 25 - Supercooled Large Drop Icing Conditions, January 1.

[4] M. Bragg, W. Perkins, N. Sarter, T. Basar, P. Voulgaris, H. Gurbacki, et al., An interdisciplinary approach to inflight aircraft icing safety, in: 36th AIAA Aerospace Sciences Meeting and Exhibit, 1998, p. 95.

[5] D. Jackson, Primary Ice Detection Certification under the New FAA and EASA Regulations, SAE Technical Paper 2015-01-2105, 2015, http://dx.doi.org/10.4271/2015-01-2105.

[6] SAE AS5498, Minimum operational performance specification for inflight icing detection systems.

[7] EUROCAE ED 103, Revision a, 2017, Minimum Operational Performance Standard for Inflight Icing Detection Systems.

[8] RTCA DO-160G, Environmental conditions and test procedures for airborne equipment.

[9] D. Jackson, J. Goldberg, Ice Detection Systems: A Historical Perspective, SAE Technical Paper 2007-01-3325, 2007, http://dx.doi.org/10.4271/2007-01-3325.

[10] B. Cheng, Y. Han, K.S. Brentner, J.L. Palacios, P. J. Morris, Quantification of rotor surface roughness due to ice accretion via broadband noise measurement, in: American Helicopter Society 70th Annual Forum Proceedings, 2014.

[11] K. Jamison, Romanweston daniel clarence heuer, 2017, Current Assignee Rosemount Aerospace Inc, US10450075B2, United States.

[12] Benjamin Wiltshire, Kiana Mirshahidi, Kevin Golovin, Mohammad H. Zarifi, Robust and sensitive frost and ice detection via planar microwave resonator sensor, Sensors Actuators B (ISSN: 0925-4005) 301 (2019) 126881, http://dx.doi.org/10.1016/j.snb.2019.126881.

[13] Q. Liu, Jen Cheng-Kuei, Wu Kuo-Ting, Kobayashi Makiko, Mrad Nezih, In-situ ice and structure thickness monitoring using integrated and flexible ultrasonic transducers, 2008.

[14] M. Tribus, M.P. Moyle, Ice Detecting Apparatus. U.S. Patent 2766619, October 16, 1953.

[15] A.V. Korolev, J.W. Strapp, G.A. Isaac, A.N. Nevzorov, The Nevzorov airborne hot-wire LWC–TWC probe: Principle of operation and performance characteristics, J. Atmos. Ocean. Technol. 15 (6) (1998) 1495–1510, http://dx.doi.org/10.4271/2007-01-3325.

[16] M. González del Val, J. Mora Nogués, P. García Gallego, M. Frövel, Icing condition predictions using FBGS, Sensors 21 (2021) 6053, http://dx.doi.org/10.3390/s21186053.

[17] M. Frovel, A.B.F.-M. Maeso, J. Mora, A. Agüero, S.sor. Mendi, R.L. Herredera, A.G.-M. Garcia, M.G. del Val, System and Method for Detecting Ice Formation on a Body, European Patent Office (EPO): WO/2020/053202, 2020, March 19, 2020.

[18] J. Zou, L. Ye, J. Ge, Ice type detection using an oblique end-face fibre-optic technique, Meas. Sci. Technol. 24 (3) (2013) 035201.

[19] Javier Martínez, Airán Ródenas, Andreas Stake, Miquel Traveria, Magdalena Aguiló, Javier Solis, Roberto Osellame, Taro Tanaka, Benoit Berton, Shigueo Kimura, Nadine Rehfeld, Francesc Díaz, Harsh-environment-resistant OH-vibrations-sensitive mid-infrared water-ice photonic sensor, Adv. Mater. Technol. WILEY (2017) http://dx.doi.org/10.1002/admt.201700085.

[20] Stanley M. Klainer, San Ramon, Fred P. Milanovich, Optical Sensor for the Detection of Ice Formation and Other Chemical Species, US Patent 4,913,519, 1990.

[21] M.W. Rothhardt, C. Chojetzki, H.R. Mueller, High-mechanical-strength single-pulse draw tower gratings, in: Proceedings of the SPIE—International Society for Optical Engineering, Vol. 5579, November, 2004, 2004, http://dx.doi.org/10.1117/12.567801.

[22] M. Frövel, Sensores de Fibra Optica Tipo Redes de Bragg Embebidos En Material Compuesto Para Medir Deformaciones Y Temperaturas Criogénicas, (Ph.D. thesis), Technical University of Madrid, Madrid, Spain, 2006.

[23] T. Ringel, T. Bosselmann, E.F. Erlangen, Field guide to nonlinear calibration of fiber bragg gratings for temperature sensors with a wide temperature range, in: AMA Conferences 2017, Nürnberg, Vol. 30, Germany, 2017.

[24] Smoothing and Differentiation of Data by Simplified Least Squares Procedures, Abraham Savitzky, M.J.E. Golay, Anal. Chem. 36 (8) (1964) 1627–1639, http://dx.doi.org/10.1021/ac60214a047.

[25] Allan Wong, Gang-Ding Peng, Applications of discrete wavelet transform in optical fibre sensing, 2011, http://dx.doi.org/10.5772/21039.

[26] Ali N. Akansu, Wouter A. Serdijn, Ivan W. Selesnick, Emerging applications of wavelets: A review, Phys. Commun. (ISSN: 1874-4907) 3 (1) (2010) 1–18, http://dx.doi.org/10.1016/j.phycom.2009.07.001.

[27] Ali Naci Akansu, Filter banks and wavelets in signal processing: a critical review, in: Proc. SPIE 1977, Video Communications and PACS for Medical Applications, Vol. 29, 1993, http://dx.doi.org/10.1117/12.160487.

[28] Fawcett Tom., Introduction to ROC analysis, Pattern Recognit. Lett. 27 (2006) 861–874, http://dx.doi.org/10.1016/j.patrec.2005.10.010.

[29] B.L. Messinger, Equilibrium temperature of an unheated icing surface as a function of air speed, J. Aeronaut. Sci. 20 (1953) 29–42.

[30] Irving Langmuir, Katharine B. Blodgett, A Mathematical Investigation of Water Droplet Trajectories, Army Air Forces Technical Report (5418), 1946.

[31] A. Samad, E. Villeneuve, C. Blackburn, F. Morency, C. Volat, An experimental investigation of the convective heat transfer on a small helicopter rotor with anti-icing and de-icing test setups, Aerospace 8 (2021) 96, http://dx.doi.org/10.3390/aerospace8040096.

[32] James Newton, G. Vanfossen, Philip Poinsatte, Kenneth Dewitt, Measurement of local convective heat transfer coefficients from a smooth and roughened NACA-0012 airfoil: Flight test data, 1988.

[33] I.H. Abbott, A.E. von Doenhoff, Theory of Wing Sections, Dover Publications, New York, NY, USA, 1959, p. 321.

[34] F. Kreith, R. Manglik, M. Bohn, Principles of Heat Transfer, seventh ed., Cengage Learning, Boston, Massachusetts, United States, 2010, pp. 420–430.
[35] K. Ignatowicz, F. Morency, H. Beaugendre, Sensitivity study of ice accretion simulation to roughness thermal correction model, Aerospace 8 (2021) 84, http://dx.doi.org/10.3390/aerospace8030084.
[36] K. Yamaguchi, R.J. Hansman, Heat transfer on accreting ice surfaces, J. Aircraft. 29 (1992) 108–113, http://dx.doi.org/10.2514/3.46132.
[37] G.A. Ruff, B.M. Berkowitz, Users Manual for the NASA Lewis Ice Accretion Prediction Code (LEWICE), NASA, Sverdrup Technology, Inc., Lewis Research Center Group Brook Park, Ohio, 1990.
[38] G. Fortin, J.-L. Laforte, A. Ilinca, Heat and mass transfer during ice accretion on aircraft wings with an improved roughness model, Int. J. Therm. Sci. 45 (2006) 595–606.
[39] W. Wright, User's Manual for LEWICE Version 3.2, NASA, Sverdrup Technology, Inc.; QSS Group, Inc., Cleveland, OH, USA, 2008.
[40] Y. Bourgault, Z. Boutanios, W.G. Habashi, Three-dimensional Eulerian approaches to droplet impingement simulations using FENSAP-ICE, Part 1: Model, algorithm, and validation, J. Aircr. 37 (1) (2000).
[41] H. Beaugendre, F. Morency, W. Habashi, FENSAP-ICE's three-dimensional in-flight ice accretion module: ICE3D, J. Aircr. 40 (2) (2003).
[42] T.H. Bond, D.N. Anderson, Manual of Scaling Methods, Technical Report, Ohio Aerospace Institute, Brook Park, OH, USA, 2004.
[43] M. Bain, J. Gayet, Contribution to the modelling of the ice accretion process: Ice density variation with the impacted surface angle, Ann. Glaciol. 4 (1983) 19–23, http://dx.doi.org/10.3189/S0260305500005176.
[44] The density and structure of ice formed by accretion, W.C. Macklin, Q. J. R. Meteorol. Soc. 88 (1962) 30–50.
[45] SAE ARP5905 Calibration and Acceptance of Icing Wind Tunnels, AC-9C Aircraft Icing Technology Committee, SAE International, 2015, http://dx.doi.org/10.4271/ARP5905, Reaffirmed on September 26.

Miguel González studied a degree in Aerospace Engineering the Technical University of Madrid, specialized on Aerospace Science and Technology with a Master Degree in Aeronautical Engineering. He did an internship in INTA about SHM, and is specialized in algorithm design for damage detection. Now he is researcher in the Metallic materials department and he is working in European Projects related with ice (SENS4ICE and SoundofIce).

Malte Frövel studied Industrial Engineering in the Technical University of Claustal and he did his phD in Aeronautics Engineering in The Technical University of Madrid with a Cum Laude grade. He was researcher in the DLR between 1990 and 1994 and after he moved to INTA in Spain.

Now he works as Research Professor of the Spanish Public Institutes and is Head of the Composite Materials Department in INTA. His area of expertise is related with Structural Health Monitoring in aircraft and damage detection in composite materials structures.